

## Synthesis of ZnO/ZnFe<sub>2</sub>O<sub>4</sub> nanocomposites in organic-free media and their photocatalytic activity under natural sunlight

Rahmayeni<sup>1,\*</sup>, Zulhadjri<sup>1</sup>, Yeni Stiadi<sup>1</sup>, Harry Agusnar<sup>2</sup> and Syukri Arief<sup>1</sup>

<sup>1</sup> Department of Chemistry, Faculty of Mathematic and Natural Sciences, Andalas University, 25163, Padang, Indonesia  
Phone: +6281363100506

<sup>2</sup> Department of Chemistry, Faculty of Mathematic and Natural Sciences, Universitas Sumatera Utara, 20155, Medan, Indonesia

**ABSTRACT** – Nanocomposite ZnO/ZnFe<sub>2</sub>O<sub>4</sub> photocatalysts with different proportions of ZnFe<sub>2</sub>O<sub>4</sub> were synthesized in organic-free media using metal nitric as precursors. The ZnO phase with hexagonal wurtzite structure and low crystallinity of ZnFe<sub>2</sub>O<sub>4</sub> was confirmed using XRD (X-Ray diffraction). Different morphologies of the nanocomposites were obtained ranging from rice grain-like with a porous surface to homogeneous sphere-like nanoparticles as shown in Scanning Electron Microscopy (SEM) and TEM Transmission Electron Microscopy (TEM) studies. Magnetic properties measured by Visible Sampler Magnetometer (VSM) showed diamagnetic and paramagnetic behavior for the nanocomposites. Analysis with Diffuse Reflectance Spectrophotometer (DRS) UV-vis showed an increase the composition of ferrite in composites increasing its ability to absorb visible light. Photocatalytic activities of ZnO/ZnFe<sub>2</sub>O<sub>4</sub> nanocomposites on the degradation of Rhodamine B dye reached 95.6% after 3 h under natural sunlight suggesting their suitability for sunlight driven photocatalytic applications.

### ARTICLE HISTORY

Revised: 22<sup>nd</sup> Aug 2019

Accepted: 23<sup>rd</sup> Apr 2020

### KEYWORDS

ZnO/ZnFe<sub>2</sub>O<sub>4</sub>;  
photocatalyst;  
organic-free media;  
natural sunlight;  
paramagnetic.

## INTRODUCTION

The semiconductor photocatalysts TiO<sub>2</sub> and ZnO are the most widely used in photocatalytic processes due to their chemical and biology stability. In recent years, the attention of researchers has been focused on ZnO because of its high photosensitivity, large excitation binding energy [1–3], low cost, and higher quantum efficiency [4, 5]. It is also environmentally friendly and naturally available [6, 7]. However, since the wide band gap of ZnO is almost the same as TiO<sub>2</sub> ( $\pm 3.37$  eV), this material absorbs well under UV light but is not effective if used with visible light [8, 9]. At ground level, solar energy comprises just 4% UV light and 50% visible light [10]. Therefore, the development of visible light-based photocatalytic compounds that can break down dyes is needed, particularly in countries such as Indonesia, which experience dye pollution problems in their waterways.

Although ZnO can utilize visible light in the photocatalytic process, its efficiency is still low. In order to increase the activity of ZnO in the visible region, various modifications including doping with metals [11, 12], nonmetallic elements [13], and metal oxides [14, 15] have been tried. In addition, another challenge exists at the separation step; the photocatalyst is still difficult to separate from the liquid [16, 17]. Spinel ferrite with the formula MFe<sub>2</sub>O<sub>4</sub> can also be used to increase the activity of ZnO [18]. Ferrite has been used to enhance the activity of TiO<sub>2</sub> in the visible light region [19]. Spinel ferrite from zinc (ZnFe<sub>2</sub>O<sub>4</sub>) is a superparamagnetic material which has a narrow band gap of about 1.97 eV. As a narrow band gap semiconductor, ZnFe<sub>2</sub>O<sub>4</sub> has the ability to utilize visible light [20–22]. However, ZnFe<sub>2</sub>O<sub>4</sub> is not effectively used alone due to the rapid recombination of electrons from the conduction band to the hole (+) [19, 23]. The combination of ZnO with ZnFe<sub>2</sub>O<sub>4</sub> will produce ZnO/ZnFe<sub>2</sub>O<sub>4</sub> a nanocomposite which can absorb visible light and has paramagnetic behavior. If the nanocomposite is used as a photocatalyst, it can be separated easily from the liquid by applying an external magnetic field [4].

Synthesis of ZnO/ZnFe<sub>2</sub>O<sub>4</sub> has been studied using different methods as reported by several researchers. ZnO/ZnFe<sub>2</sub>O<sub>4</sub> has already been synthesized by coprecipitation in NH<sub>4</sub>OH solution with activated carbon support. The resulting composite was used for degradation of wastewater under the light of a 500 Watt halogen lamp with an efficiency of up to 90% during a 120 min incubation [1]. The core-shell ZnO@ZnFe<sub>2</sub>O<sub>4</sub> catalysts synthesized by a solvothermal method using ethanol as solvent followed by precipitation were used to degrade methylene blue dye under a 6 Watt UV lamp [4]. Multi-porous nanotubes of this composite with enhanced photocatalytic activity were fabricated via a facile electrospinning and subsequent calcination process [7]. A core/shell nano cable array of this material was grown on a sapphire substrate and used for the degradation of Rhodamine B under a 150 Watt Xenon light [10]. Furthermore, sphere-like nanoparticles of the same materials were also synthesized via a solvothermal method followed by ultrasonic agitation and immobilization on graphene. These composites were used for the degradation of methylene blue under a 500 Watt Xenon lamp [16]. ZnO/ZnFe<sub>2</sub>O<sub>4</sub> particles have been synthesized by a microwave combustion method using sodium acetate (NaAc) as fuel and then used for the removal of methylene blue (MB) from an aqueous solution in a batch system [24]. Uniform ZnO/ZnFe<sub>2</sub>O<sub>4</sub> fluorescent magnetic composite hollow nanospheres were also successfully fabricated using

carbonaceous nanospheres as templates, which were synthesized via a hydrothermal approach [25]. Nevertheless, to the best of our knowledge, the fabrication of ZnO/ZnFe<sub>2</sub>O<sub>4</sub> nanocomposites by a facile method in organic-free media has not previously been reported. In this method, the material was synthesized without using hazardous chemicals at low temperatures, so it is a safe method for researchers and environmentally friendly.

In the present work, ZnO/ZnFe<sub>2</sub>O<sub>4</sub> nanocomposites were synthesized in organic-free media through a two-stage process using simple hydrothermal methods [26]. The first stage was the synthesis of ZnFe<sub>2</sub>O<sub>4</sub> and then in the second stage, ZnO/ZnFe<sub>2</sub>O<sub>4</sub> was synthesized using ZnFe<sub>2</sub>O<sub>4</sub> obtained from the first stage. The resulted nanocomposites were characterized using several instruments such as XRD, SEM, TEM, EDS, VSM, UV-vis DRS, BET, and FT-IR. These nanocomposites were used to degrade the Rhodamine B dye under natural sunlight. In this work, we also studied the influence of the ZnO:ZnFe<sub>2</sub>O<sub>4</sub> ratio and the amount of catalyst on the degradation of the dye. The photocatalytic properties of the nanocomposites were compared to those obtained from ZnO and ZnFe<sub>2</sub>O<sub>4</sub>.

## METHODS AND MATERIALS

### Materials

The following reagents and chemicals were used in this work; Zn(NO<sub>3</sub>)<sub>2</sub>·4H<sub>2</sub>O (Merck), Fe(NO<sub>3</sub>)<sub>3</sub>·9H<sub>2</sub>O (Merck), NaOH (Merck), ethanol (Merck), distilled water, and Rhodamine-B. All the chemicals were analytical grade and were used without further purification.

### Synthesis of ZnFe<sub>2</sub>O<sub>4</sub> and ZnO Nanoparticles

Nanoparticles of ZnFe<sub>2</sub>O<sub>4</sub> were synthesized in organic-free media according to the modified previous method as follows [27]; 10 mmol of Zn(NO<sub>3</sub>)<sub>2</sub>·4H<sub>2</sub>O and 20 mmol of Fe(NO<sub>3</sub>)<sub>3</sub>·9H<sub>2</sub>O as initial precursor were dissolved in 100 mL distilled water with stirring at 500 rpm. Then, NaOH (2 M) was added dropwise to adjust the pH to 12. The dark brown mixture was placed into a teflon-lined stainless steel autoclave and heated for 3 h at 180°C. After that, the autoclave was cooled at room temperature. The precipitate was collected by filtration and washed with distilled water until the pH reached 7 followed by oven drying at 100°C for 2 h. The same procedure was also used to prepare ZnO particles as a control using Zn(NO<sub>3</sub>)<sub>2</sub>·4H<sub>2</sub>O as a precursor.

### Synthesis of ZnO/ZnFe<sub>2</sub>O<sub>4</sub> Nanocomposites

ZnO/ZnFe<sub>2</sub>O<sub>4</sub> nanocomposites were synthesized using ZnFe<sub>2</sub>O<sub>4</sub> in organic-free media using a simple hydrothermal method [18]. Zn(NO<sub>3</sub>)<sub>2</sub>·4H<sub>2</sub>O and ZnFe<sub>2</sub>O<sub>4</sub> nanoparticles were mixed into 40 mL of distilled water at a mole ratio of Zn<sup>+2</sup>:ZnFe<sub>2</sub>O<sub>4</sub> of 1: 0.01, 1: 0.05, and 1: 0.1 (named NC-1, NC-2, and NC-3, respectively). The pH of the mixture was adjusted to 12 using NaOH (2 M) and then the mixture was heated at 180°C for 3 h and cooled as described above. The powder obtained was filtered and washed with distilled water until the pH dropped to 7 and then was dried at 100°C for 2 h.

### Photocatalytic Activity

The photocatalytic activity of the samples was evaluated by measuring the degradation of a Rhodamine B solution under sunlight. 20 mg of ZnO/ZnFe<sub>2</sub>O<sub>4</sub> was dispersed in 20 mL of a Rhodamine-B solution (10 ppm in distilled water). The mixture was exposed to solar irradiation for 0.5 to 3 h (11:00 am until 14:00 pm). After that, the ZnO/ZnFe<sub>2</sub>O<sub>4</sub> was removed and the absorbance of the solution was measured at 553 nm to determine the degradation percentage of Rhodamine B dye. The same procedures were performed for ZnO, ZnFe<sub>2</sub>O<sub>4</sub>, and recycled nanocomposites.

### Characterization

The crystalline phases of nanocomposites of ZnO and ferrite were identified by X-Ray diffraction (XRD Philips X'pert PANalytical PW3040). The morphology and composition of the samples were analyzed by scanning electron microscopy and energy-dispersive X-ray spectroscopy (SEM-EDX, JEOL JSM-6360LA). Transmission electron micrographs were obtained using a JEM-1400 TEM. The magnetic properties of the sample were measured by vibrating sample magnetometer (VSM OXFORD 1.2 H). The absorbance spectra of the nanocomposites were recorded using a diffuse reflectance spectrophotometer (DRS) UV-vis (Shimadzu UV-vis 2450 spectrophotometer) at room temperature. The adsorption-desorption isotherm analyses were conducted using a surface area and pore size analyzer (Quantachrome Nova 1200 E). Fourier transformed infrared (FT-IR) spectra were obtained on FT-IR Thermo Nicolet iS5 using the KBr pellet technique.

## RESULTS AND DISCUSSION

### XRD Analysis

The structure and particle size of samples were analyzed by X-ray diffractometer (XRD). Figure 1 shows the XRD patterns of ZnO, ZnFe<sub>2</sub>O<sub>4</sub>, and nanocomposites. The ZnO sample shows the specific peaks at  $2\theta = 31.7^\circ$  (hkl 100),  $34.4^\circ$  (hkl 002),  $36.2^\circ$  (hkl 101),  $47.5^\circ$  (hkl 105) and  $56.5^\circ$  (hkl 110) corresponding to the hexagonal structure of wurtzite (ICDD No.01-078-2585). For the sample of ZnFe<sub>2</sub>O<sub>4</sub>, the specific peaks are detected at  $2\theta = 29.90^\circ$  (hkl 220),  $35.17^\circ$  (hkl 311),  $42.77^\circ$  (hkl 400),  $56.5^\circ$  (hkl 511) and  $62.27^\circ$  (hkl 440) analog to the spinel cube structure (ICDD No. 00-001-1108). XRD patterns of the nanocomposites (NC) with different compositions are dominated by ZnO with a wurtzite structure. This indicates that the addition of ZnFe<sub>2</sub>O<sub>4</sub> did not change the ZnO structure in these nanocomposites. No peaks for ZnFe<sub>2</sub>O<sub>4</sub> were detected, probably due to the lower crystallinity of this phase. In addition, it can also be assumed that ZnFe<sub>2</sub>O<sub>4</sub> was covered by ZnO to form a core-shell since ZnFe<sub>2</sub>O<sub>4</sub> was only present in small amounts. For all the NC XRD patterns, there are no other peaks observed indicating no impurities in the samples. The ZnO crystal size within the nanocomposites could be calculated from the highest peaks using the Debye-Scherrer formula [4]. The average crystal size of the nanocomposites was 31.9, 33.0, and 34.4 nm for NC-1, NC-2, and NC-3, respectively.

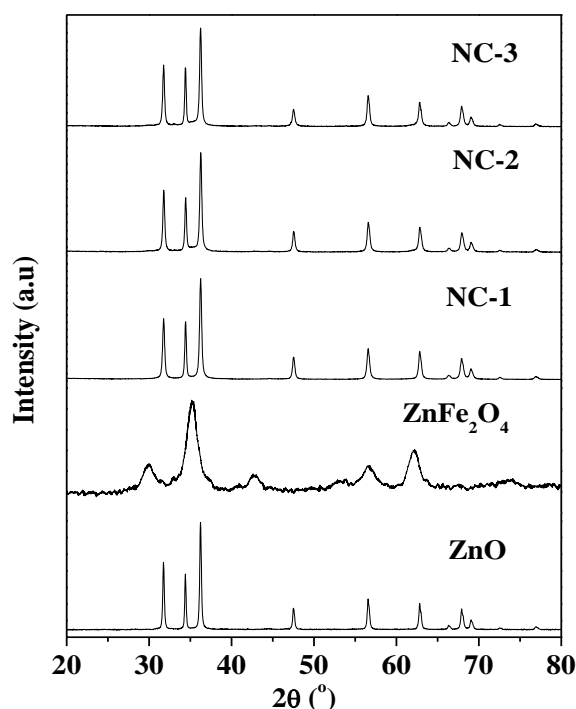


**Figure 1.** XRD patterns of ZnO, ZnFe<sub>2</sub>O<sub>4</sub>, NC-1, NC-2, and NC-3.

### Morphology of Nanocomposites

In order to investigate the surface morphology, particle size, and structure of the composites, the samples were analyzed by SEM and TEM. Figure 2 shows the SEM images of ZnFe<sub>2</sub>O<sub>4</sub> nanoparticles, NC-1, and NC-2. In Figure 2 (a-b), it can be seen that the ZnFe<sub>2</sub>O<sub>4</sub> nanoparticles were constructed of lots of homogeneous spherical-like nanoparticles with particle sizes of 30-83 nm. The surface morphology of NC-1 and NC-2 is shown in Figure 2(c-d) and (e-f), respectively. The morphology of these two nanocomposites is different from each other. The morphology NC-1 partly looks rice-like, meanwhile the NC-2 morphology more regular, fine shaped granules, porous and homogeneous with the grain size of the particles in the range of 42-83 nm. These pores will be favorable to the photocatalytic properties. The change from rice-like morphology of NC-1 to granule morphology of NC-2 was caused by the higher amount of ZnFe<sub>2</sub>O<sub>4</sub> in the later.

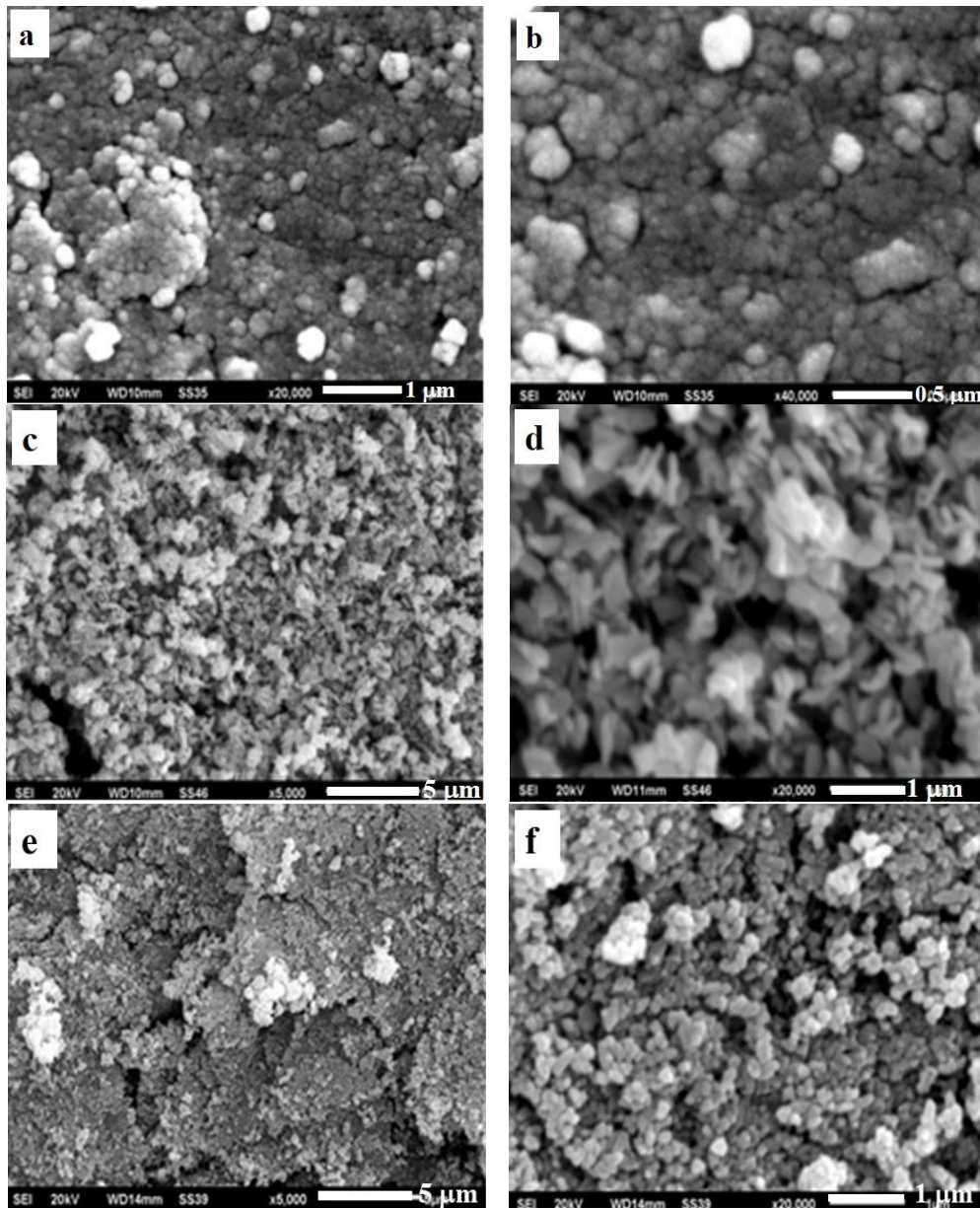


**Figure 2.** SEM Images of: (a-b)  $\text{ZnFe}_2\text{O}_4$ , (c-d) NC-1 and (e-f) NC-2.

In order to clearly understand the microstructure of the composites, the samples were analyzed by TEM. Figure 3 is the TEM image and SAED of the NC-2 sample. From panels a and b, it can be seen that this nanocomposite looks like small partly broken granules. The change from rice-like grains (NC-1) to the small granules (NC-2) can be predicted to be due to the ferrite nanoparticles of  $\text{ZnFe}_2\text{O}_4$  layered by ZnO to form the core-shell, consequently becomes larger in size [4]. This condition explains the absence of peaks from  $\text{ZnFe}_2\text{O}_4$  in the XRD analysis. In Figure 3(c) can be seen the occurrence of  $\text{ZnFe}_2\text{O}_4$  crystal diffused on the ZnO crystal and this is clearly indicating the ferrite nanoparticles dispersed on the surface of ZnO in order to form the core-shell like structure. The SAED pattern in Figure 3(d) shows the crystallinity patterns of nanocomposite noticed for polycrystalline of the spinel phase of  $\text{ZnFe}_2\text{O}_4$  and wurtzite phase of ZnO which mixed each other [8, 17].

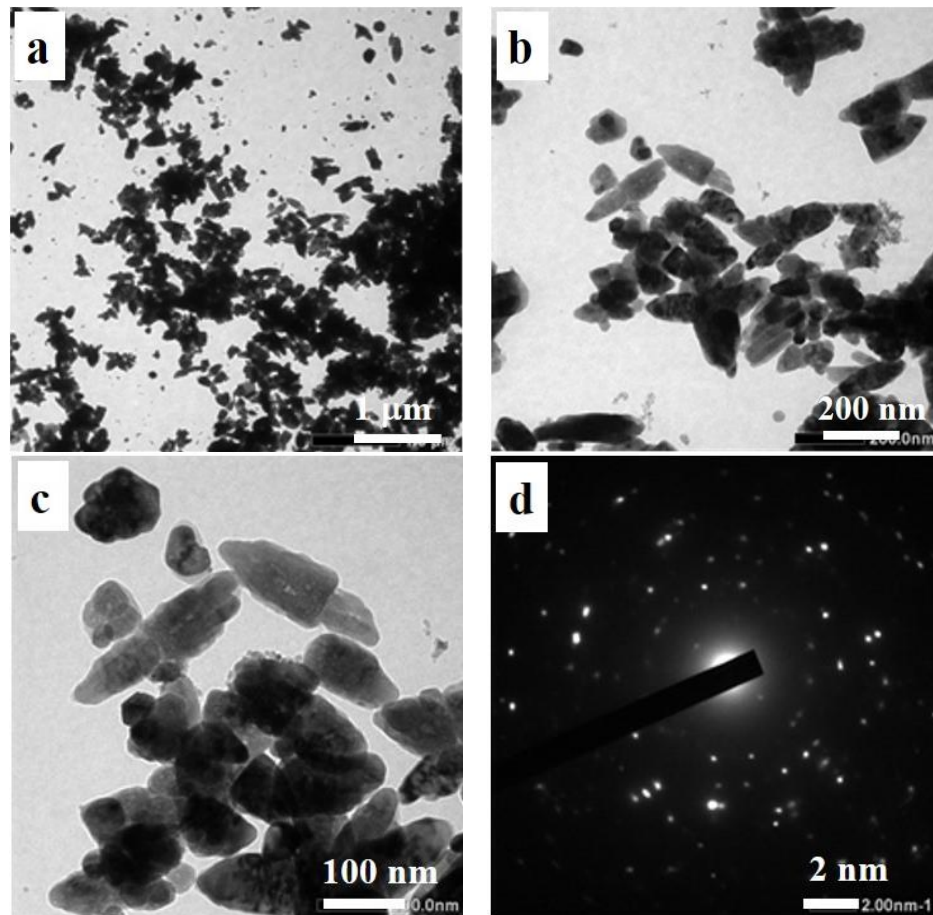


**Figure 3.** TEM image of the NC-2 at different magnifications (a-c) and SAED (d).

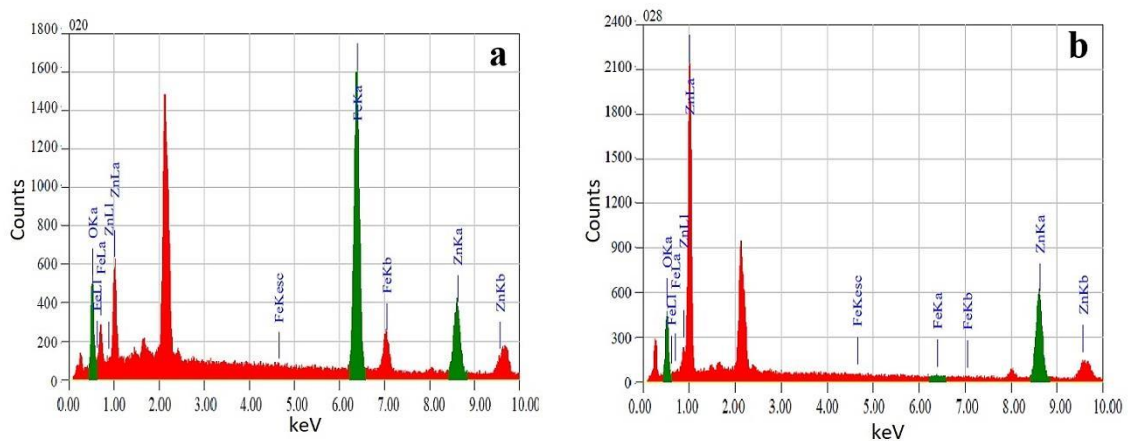


**Figure 4.** EDS spectra of (a)  $\text{ZnFe}_2\text{O}_4$  and (b) NC-2.

### EDS Analysis

The energy dispersion spectroscopy (EDS) analysis was conducted for the samples  $\text{ZnFe}_2\text{O}_4$  and NC-2 and the results are shown in Figure 4. For the  $\text{ZnFe}_2\text{O}_4$  nanoparticle (Figure 4a) the peaks of the Zn, Fe, and O elements are present without any other impurities with percentages of 32.55%, 56.65%, and 10.80%, respectively. Meanwhile, the elements contained in the NC-2 nanocomposite (Fig. 4b) consist of Zn, Fe, and O with percentages of 81.66%, 17.93%, and 0.41%, respectively. The percentages of the measured elements were in good agreement with the stoichiometry calculated results. The EDS data shows the presence of  $\text{ZnFe}_2\text{O}_4$  in the nanocomposite even though in the XRD analysis the peaks for  $\text{ZnFe}_2\text{O}_4$  were not detected.

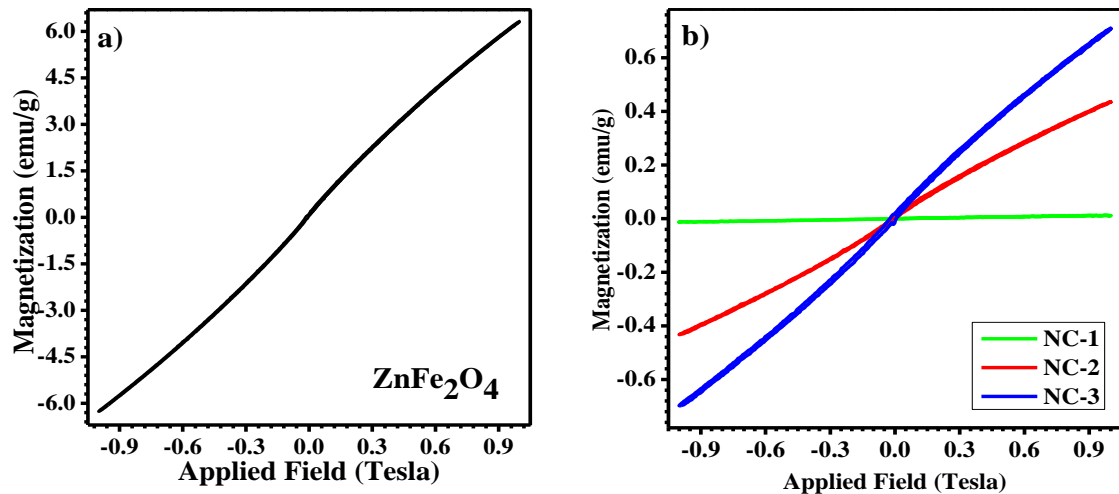


**Figure 5.** Magnetic properties of (a)  $\text{ZnFe}_2\text{O}_4$  (b) NC-1, NC-2, and NC-3.

### Magnetic Properties Analysis

Magnetic properties of the  $\text{ZnFe}_2\text{O}_4$  nanoparticles, NC-1, NC-2, and NC-3 were measured by VSM at room temperature and the results are shown in Figure 5. The magnetic saturation ( $MS$ ) value of  $\text{ZnFe}_2\text{O}_4$  nanoparticles is 6.4 emu/g (Figure 5a). This value is the same as the  $MS$  value of  $\text{ZnFe}_2\text{O}_4$  reported by [20] and described as superparamagnetic. The  $MS$  values of NC-1, NC-2, and NC-3 are 0.013 emu/g, 0.43 emu/g, and 0.7 emu/g, respectively as shown in Figure 5(b). These results correspond to diamagnetic (NC-1) and paramagnetic (NC-2 and NC-3) properties. Based on the  $MS$  values of all nanocomposites, it can be concluded that increasing the proportion of  $\text{ZnFe}_2\text{O}_4$  in nanocomposites tends to increase the magnetic properties. By observing the magnetic hysteresis curves, it is clear that the magnetic  $\text{ZnFe}_2\text{O}_4$  nanoparticles were more active than the NC due to the higher  $MS$  value. The lower  $MS$  of NCs is caused by the diamagnetic properties of ZnO which reduces the magnetic nature of the  $\text{ZnFe}_2\text{O}_4$  nanoparticles [28]. Nanocomposites with magnetic behavior have an advantage as these nanoparticles can be easily separated from the liquid by the application of an external magnetic field and can be recycled.

### DRS UV-vis Analysis

In order to investigate the optical properties, the samples were analyzed by DRS UV-vis spectroscopy. Figure 6 shows the UV-vis diffuse reflection spectra of  $\text{ZnFe}_2\text{O}_4$  and all of the nanocomposites. The spectrum of  $\text{ZnFe}_2\text{O}_4$  exhibited high absorption intensity in the visible region from 400 to 700 nm. It is known that the absorption edge for pure ZnO is below 400 nm [16]. The light absorption by the nanocomposites was high in the region below 350 nm and decreased sharply in the region above 350 to 400 nm and was then relatively constant in the visible region. An increase in the proportion of  $\text{ZnFe}_2\text{O}_4$  in the nanocomposite resulted in an increase in visible light absorption. The enhanced nanocomposite absorption in the visible light region can be attributed to the transition of electrons from the 2p orbital of O into the 3d orbital of Fe according to the energy band structure of  $\text{ZnFe}_2\text{O}_4$  doped into the nanocomposite [29].

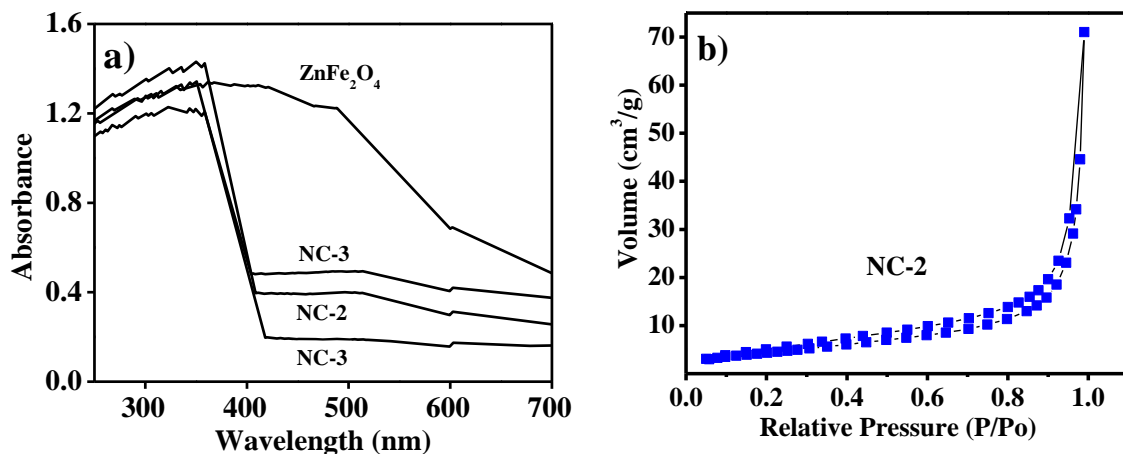


**Figure 6.** (a) DRS UV-vis spectra of NC-1, NC-2, NC-3, and  $\text{ZnFe}_2\text{O}_4$  and (b) BET graphic of NC-2.

## N<sub>2</sub> Adsorption–Desorption Isotherm Analysis

To investigate the porous structure and specific surface area, the nitrogen adsorption-desorption isotherms of the NC-2 sample were measured using the Brunauer–Emmett–Teller (BET) method (Figure 6b). BET studies revealed the specific relationship between the concentration of the adsorbate and its degree of adsorption onto the adsorbent surface. The adsorption-desorption isotherms of NC-2 are of type IV with a narrow hysteresis loop indicating a mesoporous structure of the sample (according to the IUPAC classification). The BET specific surface area of NC-2 is  $13.699 \text{ m}^2\text{g}^{-1}$  and the average pore diameter of the sample, calculated using the BJH equation, is  $30.588 \text{ \AA}$ . The increase in the adsorption branch with the sharp decline in the desorption branch is observed at  $P/P_0$  greater than 0.9 due to the capillary condensation of  $\text{N}_2$  into the mesoporous structure indicating good homogeneity of the NC-2 nanocomposites [27].

## FT-IR Analysis

FT-IR analysis is used to study the presence of functional groups in a system, inter and intramolecular interaction. FT-IR spectra of  $\text{ZnFe}_2\text{O}_4$  and NC-2 are shown in Figure 7. The band at  $425 \text{ cm}^{-1}$  can be assigned as the Zn–O stretching vibration and at  $561 \text{ cm}^{-1}$  as the stretching vibration of the Fe–O bond in  $\text{ZnFe}_2\text{O}_4$ . The vibrations of the Zn–O–Fe bond appeared at  $1347 \text{ cm}^{-1}$ . The band at around  $1630 \text{ cm}^{-1}$  could be assigned to the bending vibration of the H–O–H bond. In the FT-IR spectra of NC-2, only one broad band is observed at  $430\text{--}560 \text{ cm}^{-1}$  which can be assigned as the Zn–O vibration, it is due to the concentration of ZnO being very high. However, the vibration around  $532 \text{ cm}^{-1}$  can be attributed to the Fe–O vibration [30].

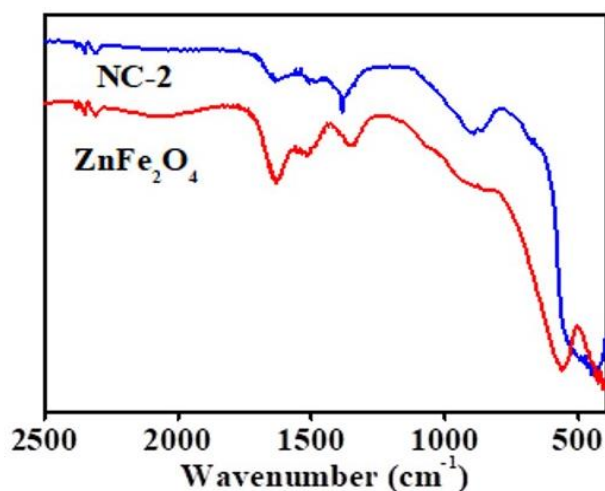
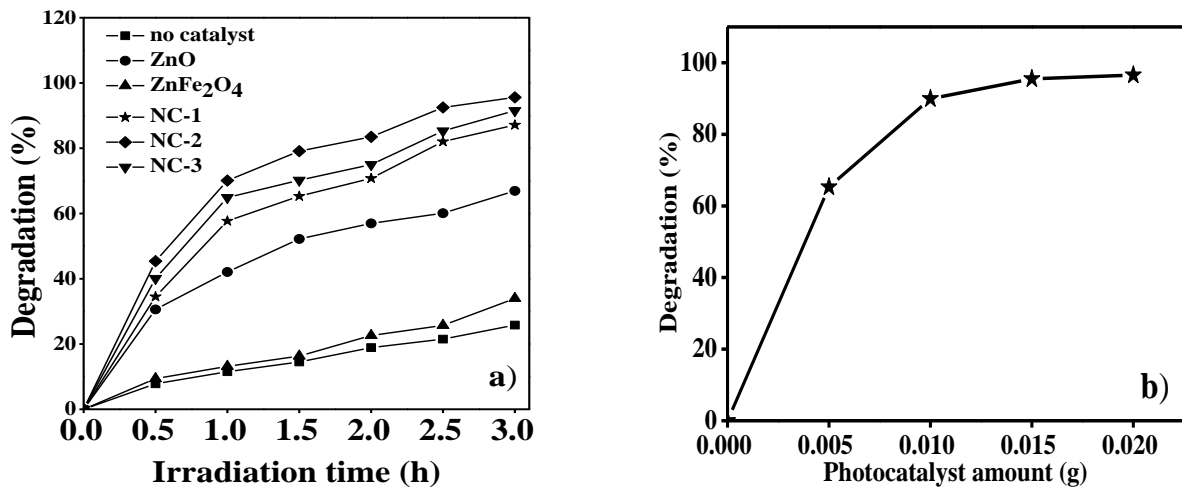


Figure 7. FT-IR analysis for  $\text{ZnFe}_2\text{O}_4$  and NC-2.

## Evaluation of Photocatalytic Activity

Rhodamine B dye was chosen to evaluate the photocatalytic activity of the as-prepared samples under natural sunlight. It is one of the dyes commonly used in the textile and food industries. The degradation of Rhodamine B dye with respect to time under natural sunlight using  $\text{ZnFe}_2\text{O}_4$ , ZnO, NC-1, NC-2, and NC-3 and in the absence of photocatalyst is shown in Figure 8(a). The evaluation was carried out from around 11:00 am to 3:00 pm.

The intensity of sunlight during the treatment was between 5120 and 6800 fc as measured using a light meter. The degradation of Rhodamine B was calculated as described previously [2, 18]. Without a catalyst, the degradation percentage of Rhodamine B dye reached only 25.8% after 3 h under natural sunlight. Using ZnO and  $\text{ZnFe}_2\text{O}_4$  catalysts unsatisfactory results were obtained as Rhodamine B was only degraded by 67% and 34%, respectively. The NC samples showed higher photocatalytic activities than ZnO and  $\text{ZnFe}_2\text{O}_4$  nanoparticles under similar conditions with the degradation percentage reaching 95.6% after 3 h using NC-2 as catalyst. The NC-1 and NC-3 also showed higher photocatalytic activity than the ZnO and  $\text{ZnFe}_2\text{O}_4$  nanoparticles; however, it was still lower than that obtained with NC-2. The higher photocatalytic activities of NC-2 as compared with other samples can be attributed to the morphology of the NC-2 being more homogeneous, porous, and with a greater surface area. These results are in agreement with the DR-UV-vis analysis shown in Figure 6 in which the absorption region for NC samples is shifted into the visible region.



**Figure 8.** (a) Degradation of Rhodamine B versus irradiation time using different catalysts and without catalyst and (b) plots of the degradation percentage of Rhodamine B versus the amount of catalyst (irradiation time is 3 h and catalyst is NC-2).

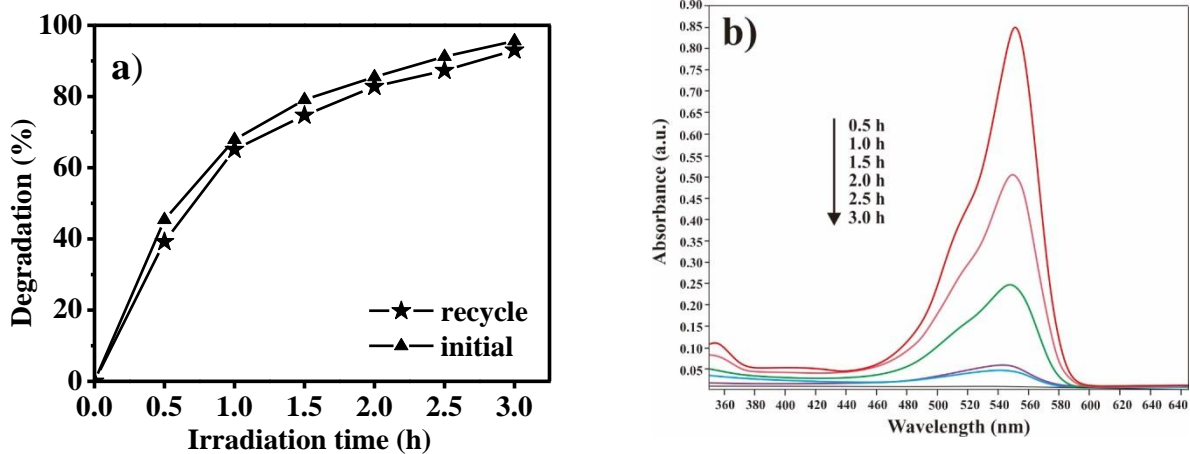


**Figure 9.** (a) Plot of degradation of Rhodamine B versus irradiation time in the presence of a fixed amount of NC-2 (0.015 g) and the recycled NC-2 (a) and (b) UV-vis absorption spectra of Rhodamine B using NC-2 photocatalyst that was exposed to sunlight for 0.5 to 3 h.

The amount of catalyst is an important parameter from the point of view of the economy for the photocatalytic reaction. To determine the effect of the amount of catalyst on photodegradation of Rhodamine B, the catalyst loading was varied from 0.005 to 0.02 g and the results are shown in Figure 8(b). The degradation percentage of Rhodamine B increased with an increasing amount of catalyst and the optimum loading was found to be 0.015 g. Adding more than 0.015 g of the catalyst did not have any significant effect on the degradation percentage of Rhodamine B. An increase in the photocatalytic activity with an increase in the amount of catalyst can be correlated with the density of active species on the surface of the catalyst. On the other hand, when an excessive amount of catalyst was used, penetration of light to the catalyst may be partially prevented and as a consequence, the photocatalytic process became slower [31].

Figure 9(a) shows the degradation percentage of Rhodamine B with fresh NC-2 and recycled NC-2 (which was already used once). Both reactions contained 0.015 g catalyst and were conducted under natural sunlight for 3 h. It can be seen that the ability of the recycled nanocomposite to degrade Rhodamine B was slightly reduced. This can be attributed to a slight agglomeration of nanocomposite particles when it was washed and dried (under a flow of air) after the first reaction. Figure 9(b) shows the UV-vis spectra of Rhodamine B solution irradiated under sunlight in the presence of NC-2 in the time range of 0.5 to 3 h. The absorption peaks decrease with an increased irradiation period and approach zero after 3 h. The absence of another peak at a different wavelength indicates that Rhodamine B was degraded into very simple compounds such as H<sub>2</sub>O and CO<sub>2</sub> [1, 7]. Thus, the photocatalytic process using ZnO/ZnFe<sub>2</sub>O<sub>4</sub> as catalyst safely degraded the dye in the wastewater without generating new waste or other dangerous derivatives.

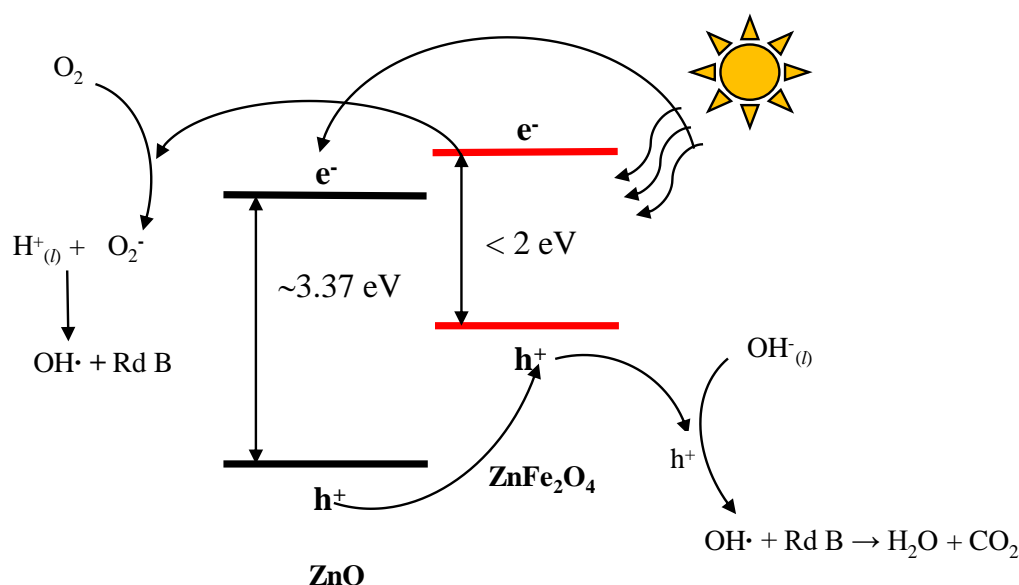


**Figure 10.** The photocatalytic mechanism proposed for dye degradation using a ZnO/ZnFe<sub>2</sub>O<sub>4</sub> nanocomposite as photocatalyst.

The mechanism of photocatalytic dye degradation using ZnO/ZnFe<sub>2</sub>O<sub>4</sub> as photocatalyst is predicted to be as shown in Figure 10. Electrons in the valence band (VB) of ZnO and ZnFe<sub>2</sub>O<sub>4</sub> will be excited to the conduction band (CB) when irradiated by sunlight and leave a positively charged hole (h<sup>+</sup>) behind [32]. The CB level of ZnFe<sub>2</sub>O<sub>4</sub> is higher than for ZnO. The difference between the band structure of ZnO and ZnFe<sub>2</sub>O<sub>4</sub> facilitates the transfer of electrons from the CB of ZnFe<sub>2</sub>O<sub>4</sub> to the CB of ZnO and migration of h<sup>+</sup> from the VB of ZnO to the VB of ZnFe<sub>2</sub>O<sub>4</sub>. This process can prevent the recombination of e<sup>-</sup> and h<sup>+</sup> pairs, so the photocatalytic activity of the nanocomposite is enhanced when it is exposed to the sunlight. After that, the generated electron will react with O<sub>2</sub> forming an O<sub>2</sub><sup>·-</sup> radical anion, which then reacts with water to form a hydroxyl radical. Hydroxyl radicals destroy the dye molecule into H<sub>2</sub>O and CO<sub>2</sub> [10, 16], [33].

## CONCLUSIONS

ZnO/ZnFe<sub>2</sub>O<sub>4</sub> nanocomposite photocatalysts with different ZnO:ZnFe<sub>2</sub>O<sub>4</sub> compositions have been synthesized in organic-free media via a two-stage process. The first stage was the synthesis of ZnFe<sub>2</sub>O<sub>4</sub> followed by the synthesis of ZnO/ZnFe<sub>2</sub>O<sub>4</sub> using the ZnFe<sub>2</sub>O<sub>4</sub> produced in the first stage. In the nanocomposites, ZnO is in a wurtzite hexagonal phase. The morphologies of the nanocomposites are either rice grain-like with a porous surface or homogeneous sphere-like. Diamagnetic and paramagnetic properties of the samples were confirmed by VSM. The nanocomposites were used to degrade Rhodamine B dye under natural sunlight irradiation and exhibited excellent photocatalytic activity. With ZnO/ZnFe<sub>2</sub>O<sub>4</sub> in composition 1:0.05 the degradation was achieved by 95% in 3 h.

## REFERENCES

- [1] H. A. Mohammed, A. Hamza, I. K. Adamu, A. Ejila, S. M. Waziri, and S. I. Mustapha, "BOD<sub>5</sub> removal from tannery wastewater over ZnO-ZnFe<sub>2</sub>O<sub>4</sub> composite photocatalyst supported on activated carbon," *J. Chem. Eng. Mater. Sci.*, vol. 4, no. 6, pp. 80–86, 2013.
- [2] L. Saikia, D. Bhuyan, M. Saikia, B. Malakar, D. K. Dutta, and P. Sengupta, "Photocatalytic performance of ZnO nanomaterials for self sensitized degradation of malachite green dye under solar light," *Appl. Catal. A Gen.*, vol. 490, pp. 42–49, 2015.
- [3] A. Khataee, M. Kiransan, S. Karaca, and S. Arefi-oshkoui, "Preparation and characterization of ZnO/MMT nanocomposite for photocatalytic ozonation of a disperse dye," *Turkish J. Chem.*, vol. 40, pp. 546–564, 2016.
- [4] R. Shao, L. Sun, L. Tang, and Z. Chen, "Preparation and characterization of magnetic core-shell ZnFe<sub>2</sub>O<sub>4</sub>@ZnO nanoparticles and their application for the photodegradation of methylene blue," *Chem. Eng. J.*, vol. 217, pp. 185–191, 2013.
- [5] Y. F. Zhu, D. H. Fan, Y. W. Dong, and G. H. Zhou, "Morphology-controllable ZnO nanostructures: Ethanol-assisted synthesis, growth mechanism and solar cell applications," *Superlattices Microstruct.*, vol. 74, pp. 261–272, 2014.
- [6] J. Xie, Y. Li, W. Zhao, L. Bian, and Y. Wei, "Simple fabrication and photocatalytic activity of ZnO particles with different morphologies," *Powder Technol.*, vol. 207, pp. 140–144, 2011.
- [7] C. Wang, X. Tan, J. Yan, B. Chai, J. Li, and S. Chen, "Electrospinning direct synthesis of magnetic ZnFe<sub>2</sub>O<sub>4</sub>/ZnO multi-porous nanotubes with enhanced photocatalytic activity," *Appl. Surf. Sci.*, vol. 396, pp. 780–790, 2017.

- [8] P. Falak, S. Hassanzadeh-Tabrizi, and A. Saffar-Teluri, "Synthesis, Characterization, and Magnetic Properties of ZnO-ZnFe<sub>2</sub>O<sub>4</sub> Nano-particles with High Photocatalytic Activity," *J. Magn. Mater.*, vol. 441, pp. 98–104, 2017.
- [9] J. Zheng, X. Song, X. Liu, W. Chen, Y. Li, and J. Guo, "Synthesis of hexagonal CoFe<sub>2</sub>O<sub>4</sub>/ZnO nanoparticles and their electromagnetic properties," *Mater. Lett.*, vol. 73, pp. 143–146, 2012.
- [10] X. Guo, H. Zhu, and Q. Li, "Visible-light-driven photocatalytic properties of ZnO/ZnFe<sub>2</sub>O<sub>4</sub> core/shell nanocable arrays," *Appl. Catal. B Environ.*, vol. 160–161, pp. 408–414, 2014.
- [11] P. Dhiman, J. Chand, A. Kumar, R. K. Kotnala, K. Mujasam, and M. Singh, "Synthesis and characterization of novel Fe@ZnO nanosystem," *J. Alloys Compd.*, vol. 578, pp. 235–241, 2013.
- [12] H. Yu et al., "Facile synthesis of Au/ZnO nanoparticles and their enhanced photocatalytic activity for hydroxylation of benzene," *Bull. Mater. Sci.*, vol. 36, no. 3, pp. 367–372, 2013.
- [13] V. Kumari, A. Mittal, J. Jindal, S. Yadav, and N. Kumar, "S-, N- and C-doped ZnO as semiconductor photocatalysts: A review," *Front. Mater. Sci.*, vol. 13, pp. 1–22, 2019.
- [14] M. Giahi, N. Badalpoor, S. Habibi, and H. Taghavi, "Synthesis of CuO/ZnO Nanoparticles and Their Application for Photocatalytic Degradation of Lidocaine HCl by the Trial-and-error and Taguchi Methods," *Bull. Korean Chem. Soc.*, vol. 34, no. 7, pp. 2176–2182, 2013.
- [15] R. Lamba, A. Umar, S. K. Mehta, and S. K. Kansal, "CeO<sub>2</sub>-ZnO hexagonal nanodisks: Efficient material for the degradation of direct blue 15 dye and its simulated dye bath effluent under solar light," *J. Alloys Compd.*, vol. 620, pp. 67–73, 2015.
- [16] L. Sun, R. Shao, L. Tang, and Z. Chen, "Synthesis of ZnFe<sub>2</sub>O<sub>4</sub>/ZnO nanocomposites immobilized on graphene with enhanced photocatalytic activity under solar light irradiation," *J. Alloys Compd.*, vol. 564, pp. 55–62, 2013.
- [17] P. Sathishkumar, N. Pugazhenthiran, R. V. Mangalaraja, A. M. Asiri, and S. Anandan, "ZnO supported CoFe<sub>2</sub>O<sub>4</sub> nanophotocatalysts for the mineralization of Direct Blue 71 in aqueous environments," *J. Hazard. Mater.*, vol. 252–253, pp. 171–179, 2013.
- [18] Rahmayeni, A. Ramadani, Y. Stiadi, N. Jamarun, and S. Arief, "Photocatalytic Performance of ZnO-ZnFe<sub>2</sub>O<sub>4</sub> Magnetic Nanocomposites on Degradation of Congo Red Dye under Solar Light Irradiation," *J. Mater. Environ. Sci.*, vol. 8, no. 5, pp. 1634–1643, 2017.
- [19] Rahmayeni, S. Arief, Y. Stiadi, R. Rizal, and Zulhadjri, "Synthesis of Magnetic Nanoparticles of TiO<sub>2</sub>-NiFe<sub>2</sub>O<sub>4</sub>: Characterization and Photocatalytic Activity on Degradation of Rhodamine B," *Indones. J. Chem.*, vol. 12, no. 3, pp. 229–234, 2012.
- [20] R. Rameshbabu, R. Ramesh, S. Kanagesan, A. Karthigeyan, and S. Ponnusamy, "Synthesis of superparamagnetic ZnFe<sub>2</sub>O<sub>4</sub> nanoparticle by surfactant assisted hydrothermal method," *J. Mater. Sci. Mater. Electron.*, vol. 24, pp. 4279–4283, 2013.
- [21] N. G. Yadav, L. S. Chaudhary, P. A. Sakhare, T. D. Dongale, P. S. Patil, and A. D. Sheikh, "Impact of Collected Sunlight on ZnFe<sub>2</sub>O<sub>4</sub> Nanoparticles for Photocatalytic Application," *J. Colloid Interface Sci.*, vol. 527, pp. 289–297, 2018.
- [22] X. Li, Y. Hou, Q. Zhao, W. Teng, X. Hu, and G. Chen, "Capability of novel ZnFe<sub>2</sub>O<sub>4</sub> nanotube arrays for visible-light induced degradation of 4-chlorophenol," *Chemosphere*, vol. 82, pp. 581–586, 2011.
- [23] G. Tong, F. Du, W. Wu, R. Wu, F. Liu, and Y. Liang, "Enhanced reactive oxygen species (ROS) yields and antibacterial activity of spongy ZnO/ZnFe<sub>2</sub>O<sub>4</sub> hybrid micro-hexahedra selectively synthesized through a versatile glucose-engineered coprecipitation/annealing process," *J. Mater. Chem. B*, vol. 1, pp. 2647–2657, 2013.
- [24] J. Feng et al., "Synthesis of Magnetic ZnO/ZnFe<sub>2</sub>O<sub>4</sub> by a Microwave Combustion Method, and Its High Rate of Adsorption of Methylene Blue," *J. Colloid Interface Sci.*, vol. 438, pp. 318–322, 2015.
- [25] H. Qian et al., "ZnO/ZnFe<sub>2</sub>O<sub>4</sub> Magnetic Fluorescent Bifunctional Hollow Nanospheres : Synthesis, Characterization, and Their Optical/Magnetic Properties," *J. Phys. Chem. C*, vol. 114, no. 41, pp. 17455–17459, 2010.
- [26] I. Kustiningsih, Sutinah, M. Stefirizky, Slamet, and W. W. Purwanto, "Optimization of TiO<sub>2</sub> nanowires synthesis using hydrothermal method for hydrogen production," *J. Mech. Eng. Sci.*, vol. 12, no. 3, pp. 3876–3887, 2018.
- [27] H. Zhu, R. Jiang, Y. Fu, R. Li, J. Yao, and S.-T. Jiang, "Novel multifunctional NiFe<sub>2</sub>O<sub>4</sub>/ZnO hybrids for dye removal by adsorption, photocatalysis and magnetic separation," *Appl. Surf. Sci.*, vol. 369, pp. 1–10, 2016.
- [28] T. J. Castro, S. W. Silva, F. Nakagomi, N. S. Moura, A. F. Jr, and P. C. Morais, "Structural and magnetic properties of ZnO-CoFe<sub>2</sub>O<sub>4</sub> nanocomposites," *J. Magn. Mater.*, vol. 389, pp. 27–33, 2015.
- [29] X. Zhu et al., "Facile synthesis, structure and visible light photocatalytic activity of recyclable ZnFe<sub>2</sub>O<sub>4</sub>/TiO<sub>2</sub>," *Appl. Surf. Sci.*, vol. 319, pp. 83–89, 2014.
- [30] S. D. Kulkarni, S. Kumbhar, S. G. Menon, K. S. Choudhari, and C. Santhosh, "Magnetically Separable core-shell ZnFe<sub>2</sub>O<sub>4</sub>@ZnO Nanoparticles for Visible Light photodegradation of methyl orange," *Mater. Res. Bull.*, vol. 77, pp. 70–77, 2016.
- [31] X. Wang, X. Wan, X. Xu, and X. Chen, "Facile fabrication of highly efficient AgI/ZnO heterojunction and its application of methylene blue and rhodamine B solutions degradation under natural sunlight," *Appl. Surf. Sci.*, vol. 321, pp. 10–18, 2014.
- [32] N. A. Amenaghawon, J. O. Osarumwense, F. A. Aisien, and O. K. Olaniyan, "Preparation and investigation of the photocatalytic properties of periwinkle shell ash for tartrazine decolorisation," *J. Mech. Eng. Sci.*, vol. 7, pp. 1070–1084, 2014.
- [33] R. Bayat, P. Derakhshi, R. Rahimi, A. A. Safekordi, and M. Rabbani, "A magnetic ZnFe<sub>2</sub>O<sub>4</sub>/ZnO/perlite nanocomposite for photocatalytic degradation of organic pollutants under LED visible light irradiation," *Solid State Sci.*, vol. 89, pp. 167–171, 2019.